WILEY-VCH

DOI: 10.1002/(**adma.202002811**)
Article type: Communication

In search of chiral molecular superconductors: κ-[(*S*,*S*)-DM-BEDT-TTF]$_2$ClO$_4$ revisited

Nabil Mroweh, Cécile Mézière, Flavia Pop, Pascale Auban-Senzier, Pere Alemany, Enric Canadell,* and Narcis Avarvari**

Dr. N. Mroweh, C. Mézière, Dr. F. Pop, Dr. N. Avarvari
MOLTECH-Anjou, UMR 6200, CNRS, UNIV Angers
2 bd Lavoisier, 49045 ANGERS Cedex, France
E-mail: flavia.pop@univ-angers.fr; narcis.avarvari@univ-angers.fr
Dr. P. Auban-Senzier
Laboratoire de Physique des Solides, Université Paris-Saclay
CNRS UMR 8502, 91405 Orsay, France
Prof. P. Alemany
Departament de Ciència de Materials i Química Física and Institut de Química Teòrica i Computacional (IQTCUB)
Universitat de Barcelona, Martí i Franquès 1, Barcelona 08028, Spain
Dr. E. Canadell
Institut de Ciència de Materials de Barcelona (CSIC)
Campus de la UAB, E-08193 Bellaterra, Spain
E-mail: canadell@icmab.es

Keywords: chirality, superconductivity, molecular conductors, band structures

The relationship between chirality and superconductivity is an intriguing question. The two enantiomeric crystalline radical cation salts κ-[(*S*,*S*)-DM-BEDT-TTF]$_2$ClO$_4$ and κ-[(*R*,*R*)-DM-BEDT-TTF]$_2$ClO$_4$, showing κ-type arrangement of the organic layers, are investigated in search for superconducting chiral molecular materials following a 1992 report indicating the occurrence of a superconducting transition in the former compound. While the initial interpretation is presently challenged through in-depth temperature and pressure dependent single crystal resistivity measurements combined with band structure calculations, the two chiral conductors show metal like behaviour with room temperature conductivities of 10-30 S cm^{-1} at ambient pressure and stabilization of the metallic state down to the lowest temperatures under moderate pressures. Moreover, their structural and theoretical investigations reveal an original feature, namely the existence of two different κ layers with

1D and 2D electronic dimensionality, respectively, as a consequence of an inter-layer charge transfer. The resistivity drop observed for one sample below 1 K and insensitive to magnetic field, possibly results from mixing in-plane and out-of-plane contributions to the measured resistance and suggests current induced charge order melting. This feature contradicts the occurrence of superconductivity in these chiral molecular conductors and leaves open the discovery of the first chiral molecular superconductors.

The quest for chiral molecular conductors[1] started in the middle of the eighties with the synthesis by Dunitz and Wallis of the first enantiopure tetrathiafulvalene (TTF) precursor, namely the (*S*,*S*,*S*,*S*) enantiomer of tetramethyl-bis(ethylenedithio)-TTF (TM-BEDT-TTF, **Figure 1**a),[2] together with the preparation of several chiral conducting salts.[3] The dimethylated precursor DM-BEDT-TTF (Figure 1a), containing only two stereogenic centres, was reported a few years later by Zambounis for the (*S*,*S*) enantiomer[4] and by Sugawara and Kawada for the (*R*,*R*).[5,6] The latter also described in the same report the (*R*,*R*,*R*,*R*) enantiomer of TM-BEDT-TTF.[5] While at that period chiral conductors were considered mostly from a chemical and crystallographic point of view as a means of variation of the library of available precursors for organic metals and superconductors, crystal packing issues and decrease of the structural disorder due to the flipping of the ethylene bridge in BEDT-TTF based conductors, their interest was revived and put in a new light thanks especially to the first experimental observations of the electrical magnetochiral anisotropy (eMChA) effect by Rikken.[7,8] This phenomenon, translating the direct influence of chirality on the electron transport properties measured in a longitudinal magnetic field, together with other indirect chirality triggered effects, such as the modulation of the structural disorder[9,10] or induction of different crystal packing between the enantiopure and racemic forms resulting in different conducting properties,[11] highly motivated intense efforts in the search of new chiral TTF precursors and conducting salts.[12] Accordingly, besides conducting salts with TM-BEDT-

TTF[13–16] and DM-BEDT-TTF,[17,18] the new enantiopure EDT-TTF based donors dimethyl-ethylenedithio-TTF (DM-EDT-TTF, Figure 1a)[19] and, very recently, methyl-EDT-TTF (Me-EDT-TTF, Figure 1a),[20] together with derived radical cation salts, have been prepared, culminating with the $(DM\text{-}EDT\text{-}TTF)_2ClO_4$ salts which allowed the first observation of the eMChA effect in a bulk chiral crystalline material.[21]

In this respect, particularly interesting is the recent observation of enhanced non-reciprocal charge transport in the superconducting state of the non-centrosymmetrical inorganic materials WS_2 nanotubes[22] and MoS_2 thin crystals.[23] Chiral superconductors are very intriguing since the degeneracy between electrons associated with *k* and *–k* wavevectors, i.e. the essential components of the Cooper pairs, is broken under magnetic field because of the electrical magnetochiral anisotropy. Besides, chiral superconductivity stimulates increasing endeavour in view of the exotic properties and functionalities that are predicted or observed, such as spontaneous generation of magnetic fields,[24] superconducting diodes[23] or quantum computing.[25] However, all these studies concern purely inorganic materials which, when they are obtained in crystalline forms, happen to crystallize in non-centrosymmetric structures,[26,27] yet this feature is impossible to predict as the initial components do not contain any chiral bias such as a stereogenic centre. Moreover, the two enantiomorphic forms and the racemate are hardly accessible in order to investigate and compare their properties in the superconducting state. As a consequence, the access to molecular chiral superconductors starting from enantiopure precursors with controlled chirality is of huge interest. We have therefore decided to explore the mixed valence salt κ-$[(S,S)\text{-}DM\text{-}BEDT\text{-}TTF]_2ClO_4$ together with its (*R,R*) enantiomer, since the former is, paradoxically when considering the numerous examples of BEDT-TTF based superconductors,[28] the only chiral organic conductor to date claimed to show superconductivity, as described by Zambounis *et al.* back in 1992.[29] However, puzzling enough, no further report from the same group or others confirmed this initial statement, in spite of a result of fundamental importance in the fields of

superconductivity and chirality. We describe herein the synthesis, structural characterization, conducting properties and in-depth extended Hückel and DFT band structure calculations of both enantiomers of κ-[DM-BEDT-TTF]$_2$ClO$_4$.

The two enantiomers (*S*,*S*) and (*R*,*R*) of DM-BEDT-TTF (Figure 1a) have been prepared according to the literature,[5,18] and then they were engaged in electrocrystallization, first in the experimental conditions described in the original paper,[29] that is in THF at room temperature (the temperature was not indicated though) under a current of 3 μA in the presence of (*n*-Bu$_4$N)ClO$_4$ as supporting electrolyte. In spite of numerous trials we did not obtain any crystalline compounds for either of the enantiomers, which determined us to slightly vary the donor/anion ratio, the temperature and current intensity. Performing the experiment at 3 °C with a current intensity of 0.5 μA (details in the ESI) eventually allowed us to obtain black crystalline plates of both enantiomeric salts. Single crystal X-ray analyses were in agreement with the reported unit cell parameters for the κ-[(*S*,*S*)-DM-BEDT-TTF]$_2$ClO$_4$ phase, the crystalline space group being the monoclinic non-centrosymmetric $P2_1$ (Table S1, ESI). The original structure, for which the reliability factor was rather high, i.e. 13.3%, was measured at room temperature (*RT*). While the authors pointed out that the perchlorate ions were disordered, they omitted to mention that in the asymmetric unit there are four independent donor molecules, hereafter noted **A**-**D**, and two anions, therefore the actual stoichiometry is 4:2 and not 2:1 (Figure 1b for the (*R*,*R*) and Figure S1 for the (*S*,*S*) enantiomers). We have measured our structures both at *RT* and *T* = 150 K with similar results. Expected differences between the two measurements, such as volume decrease due to thermal contraction and better defined ellipsoids for some atoms at 150 K, have been observed but no disorder for either the anions or the ethylene bridges. Moreover, the reliability factors and Flack parameters for the structures at 150 K are indicating the high quality X-ray diffraction data for both enantiomers (see the ESI).

As discussed by Zambounis *et al.*,[29] the most striking structural feature of this salt is the κ-type arrangement of the donors (Figure S2-S5, ESI). However, a detail of utmost importance that has been overlooked in the original report is the existence of *two different κ-type layers* formed either by **A**-**B** dimers (layer 1) or by **C**-**D** dimers (layer 2) (**Figure 2**a for layer 1, layer 2 is formed by **C**-**D** dimers and shows the same architecture, *vide infra*). The C=C and internal C–S bond lengths values are rather similar for the four **A**-**D** donors (Table S2, ESI) and do correspond to a mixed valence state. While very few BEDT-TTF salts containing two different alternating layer types such as α-κ[30] and α-"pseudo-κ"[31] have been described, those possessing two different κ layers are exceptionally rare and present potentially huge interest with respect to their electronic structures. As a matter of fact, to the best of our knowledge, there is only one reported example of such material and it concerns the κ-(BEDT-TTF)$_4$PtCl$_6$•C$_6$H$_5$CN salt which shows a very weakly activated conductivity down to 250 K where a first order phase transition takes place towards an insulating regime.[32] In that case it was proposed that the two different κ-layers[33] in the temperature range before the phase transition contain BEDT-TTF molecules in three different oxidation states.[34]

In our enantiopure salts κ-(DM-BEDT-TTF)$_4$(ClO$_4$)$_2$ every layer is built from two different donors **A**/**B** (layer 1, Figure 2a) or **C**/**D** (layer 2), making identical **A**-**B** or **C**-**D** dimers. There are six different intermolecular interactions in every layer (Figure 2a). Every dimer (interaction I) makes chains of dimers along the vertical axis *b*, through interaction II, and these chains are connected through four interactions: III / IV at one side of the chain and V / VI at the other side. To understand the electronic structure and transport properties of these salts we need to have a hint on the strength of the HOMO···HOMO interactions since there are the HOMO bands which are going to be partially emptied. This may be done by looking at the absolute value of the so-called HOMO···HOMO interaction energy,[35] $\beta_{HOMO-HOMO}$,

associated with each interaction. The calculated values for the six interactions in the two different layers of the two pure enantiomeric salts are reported in Table 1.

The calculated values of Table 1 clearly show that from the viewpoint of the HOMO···HOMO interactions (i) the salts of the two enantiomeric donors are practically identical and (ii) the two layers of the same salt exhibit noticeable differences. This is further confirmed when looking at the HOMO energies of the different donors. Whereas the difference between those of dimers **C**-**D** is practically nil (~ 0.001 eV in both the (*R*,*R*) and (*S*,*S*) salts) the difference is clear between those of dimers **A**-**B** (~ 0.030 eV in the (*R*,*R*) salt and ~ 0.090 eV in the (*S*,*S*) salt). Even if keeping the general topology of the band structure for κ phases, the difference between the two types of layers leads to marked differences in their band structures (Figure 2b top). Whereas the two upper HOMO bands, which are partially filled, are almost degenerate along one of the borders of the Brillouin zone (X-M line in Figure 2b top) for the type 2 layers, they are substantially separated for the type 1 layers. For a κ-type layer with one type of dimer as in the present salts, the separation of these two bands along this line depends on the values of the transfer integrals relating the dimers of different chains. When these interactions become very similar on both sides of the chain the two bands tend to collapse. As the values in Table 1 show, the interactions at both sides of the chains (III/IV *vs* V/VI) are very similar in type 2 layers but markedly different in those of type 1. Thus, it is understandable that the bands of layer 1 are well separated along X-M in Figure 2b (top left) whereas those of layer 2 are not (Figure 2b top right).

The Fermi surfaces calculated assuming an equal partition of the four holes between the two layers exhibit some important differences (Figure 2b bottom). Whereas that of layer 2 (Figure 2b bottom right) exhibits the typical shape for κ salts, a series of overlapping almost circular sections and thus leading to formally open and closed portions separated by a small gap, that

of layer 1 exhibits a different closed part, which looks as a rounded square (Figure 2b bottom left).

As noted before[36] this kind of Fermi surface occurs in κ phases when the donor layer becomes more one-dimensional (1D) along the direction of the donor chains. Such change in the shape of the closed portion of the Fermi surface is related to the fact that the Fermi level cuts the lower partially filled band very close to the Γ point (Figure 2b top left). Obviously, a very small electron transfer towards layer 2 would shift the Fermi level below this band at Γ and the initially closed portion would disappear to become a warped line, something that may strongly affect the physical behavior. The two salts share all the mentioned features of the electronic structure (Figure S6 and S7, ESI, for the band structure and Fermi surface of [(*S*,*S*)-DM-BEDT-TTF]$_2$ClO$_4$). Consequently, the question of the possible inter-layer charge transfer becomes a key issue in understanding the electronic structure of these salts.

Under such conditions only first-principles approaches treating on the same foot all components of the system and taking explicitly into account the interaction between donor and anion layers may lead to a correct description of the system. Thus, we have carried out a DFT study of the two salts. The calculated band structure for [(*R*,*R*)-DM-BEDT-TTF]$_2$ClO$_4$ is shown in Figure 2c top. Among the four partially filled bands (in the full calculation the bands of the two different layers superpose) it is clear that two of them are clearly separated along the X-M line whereas the other two are much less. The first pair is associated with layer 1 whereas the second is associated with layer 2. The important feature of Figure 2c top is that at Γ the Fermi level lies below the bottom part of the second band of layer 1 so that the closed part of the Fermi surface originating from layer 1 must have disappeared. The calculated DFT Fermi surface is shown in Figure 2c bottom where the portions associated with layers 1 and 2 are shown in blue and red, respectively. Whereas the contribution of layer 2 is that typical of κ phases with the open and closed portions separated by a small gap, that of layer 1 is made of

two open and warped lines perpendicular to the direction of the chains of dimers. All these results are shared by the two salts (Figure S8, ESI). Thus, (*R*,*R*)- and [(*S*,*S*)-DM-BEDT-TTF]$_2$ClO$_4$ contain two structurally similar but electronically very different donor layers with different dimensionality.

In order to further characterize the electronic structure of these phases we have evaluated the density of holes for each of the four donor molecules by integrating the associated projected density of states of the four partially filled bands. We obtained the values +0.62 (donor **A**), +0.58 (donor **B**), +0.39 (donor **C**) and +0.41 (donor **D**) for [(*R*,*R*)-DM-BEDT-TTF]$_2$ClO$_4$, and +0.63 (donor **A**), +0.57 (donor **B**), +0.40 (donor **C**) and +0.40 (donor **D**) for [(*S*,*S*)-DM-BEDT-TTF]$_2$ClO$_4$. Consequently, there is almost no charge difference between the two donors **C**-**D** of layer 2, only a slight charge transfer of +(0.04-0.06) between the two donors **A**-**B** of layer 1 and an important transfer of holes from layer 2 to layer 1 amounting to ~ 0.20 e. Thus, the bands of layer 1 are raised in energy and considerably depopulated mostly because of the asymmetry in the interactions between the chains of dimers so that the lowest band contribution to the Fermi surface evolves from closed to open. In contrast, the similarity of the interactions at both sides of the dimer chains of layer 2 keeps the typical shape of the Fermi surface for κ phases, with both closed and open contributions separated by a small gap. It is worth noting that if the hole transfer between layers is taken into account in the extended Hückel calculations, the correct Fermi surfaces are obtained (Figure S9).

In summary, both the asymmetry in the interactions between chains of dimers and the important transfer of holes between the two types of layers work together to make the electronic structure of the two layers in κ-[(*R*,*R*)-DM-BEDT-TTF]$_2$ClO$_4$ and κ-[(*S*,*S*)-DM-BEDT-TTF]$_2$ClO$_4$ considerably different. Although some portions of the Fermi surface associated with layer 1 exhibit nesting, a large part of the Fermi surface would remain unaffected so that the metallic state of the present salts should be kept until low temperatures. In addition, the electronic structure of the two layers is different enough so as to make the

simultaneous electron localization in the two layers (which in addition have a non-integer number of electrons per layer), in principle, unlikely.

With the two crystalline enantiomeric materials in our hands, we set out to measure single crystal resistivity in order to track down the superconducting transition. Careful temperature dependent in-plane resistivity measurements at various pressures have been performed on several single crystals of each enantiomer. Since no abrupt decrease of resistivity has been observed for any of the investigated temperature range and pressures, we can safely conclude that, contrary to what was claimed in the 1992 report,[29] there is no indication of the occurrence of superconductivity in this compound (**Figure 3**a,b and Figure S10-S13, ESI). Both enantiomeric compounds are weakly metallic at ambient pressure down to 80 K, with a room temperature in-plane conductivity of 10-30 S cm^{-1} (the large range of values could be related to an anisotropy of the conductivity within the plane) and then a smooth metal to insulator (MI) transition occurs. Upon applying pressure the metallic regime is steadily stabilized down to the lowest temperatures, yet a small localization still occurs below 10 K at pressures as high as 14.5 kbar. This behavior strikingly differs from the one described in 1992.[29] First, the room temperature conductivity at ambient pressure was 0.05 S cm^{-1}, which is two orders of magnitude lower than in our case, and therefore could be tentatively assigned to an out-of-plane value (*vide infra*). Then, the weakly metallic conductivity down to 75 K followed by a MI transition observed at ambient pressure is comparable to our results, but the evolution under pressure is quite different. Unexpectedly, the insulating behavior was reinforced under pressures up to 10 kbar in the high temperature regime and was followed below 35 K by a sharp decrease of the resistivity. Structure determinations and DFT calculations (*vide supra*) suggest that in-plane transport data should combine 1D conduction in layers 1 and 2D conduction in layers 2 and their contributions are expected to vary differently with the temperature. In our experiments the room temperature in-plane conductivity shows a linear dependence with the pressure with a rate between +20 and

+30%/kbar for both enantiomers (Figure S14-S15, ESI), as expected for 1D or 2D molecular metals. We have also checked the perpendicular (out-of-plane) resistivity ρ_{perp} for κ-[(*S*,*S*)-DM-BEDT-TTF]$_2$ClO$_4$ at ambient pressure. Its room temperature value is more than two orders of magnitude higher than the in-plane value and its temperature dependence is nearly proportional to in-plane data (Figure S16, ESI). This feature is commonly observed in 2D κ phases of BEDT-TTF salts.

However, for one of the crystals of [(*S*,*S*)-DM-BEDT-TTF]$_2$ClO$_4$ (#2) we observed a sharp MI transition below 80 K which is even preserved under a moderate pressure (Figure S11, ESI). This is reminiscent of a charge density wave transition typical of 1D conductors[37] or a charge ordering transition. The presence of steps on the large faces of the crystal or defects generated by microcracks during cooling down could imply a mixing of in-plane and out-of-plane contributions to the measured resistance. Moreover, amazingly, within this insulating regime, a variation of the current intensity (in the μA range) induced a sudden decrease of the resistance from several kΩ to nearly 0 at very low temperatures (Figure 3c), very much alike to the resistivity drop reported by Zambounis *et al.* in 1992,[29] which was tentatively assigned to a superconducting transition. Nevertheless, this phenomenon is not suppressed under magnetic field (Figure 3d), an argument which is against the occurrence of a superconducting state. Actually, this behavior reminds the current-induced melting of a charge ordered state, observed, for example, in the case of the so-called organic thyristors *θ*-(BEDT-TTF)$_2$CsM(SCN)$_4$ (M = Co, Zn) exhibiting giant non-linear conduction at low temperatures,[38,39] or in the (EDT-TSF)$_2$GaCl$_4$ phase.[40]

The recent observation of the electrical magnetochiral anisotropy in a bulk chiral molecular conductor reopened the longstanding question of the relationship between chirality and superconductivity in bulk materials. This is especially attractive in the case of molecular conductors because of the many ways to tune their electronic structures and to control the

absolute configuration. In this work we have prepared by electrocrystallization and thoroughly analyzed the two enantiomeric radical cation salts κ-[(*S*,*S*)-DM-BEDT-TTF]$_2$ClO$_4$ and κ-[(*R*,*R*)-DM-BEDT-TTF]$_2$ClO$_4$, the former being previously described as possibly undergoing a transition towards a superconducting state under pressure,[29] although not confirmed later on by additional investigations. Single crystal diffraction on our materials revealed an original type of packing consisting of two different κ-layers formed of orthogonal dimers of crystallographically distinct donors. Band structure calculations suggest that these salts are very unusual because of the charge transfer between different cationic layers. As a result, the different layers have also a different electronic dimensionality (1D and 2D) which is unprecedented in κ-phases. Single crystal resistivity measurements showed weakly metallic conductivity at ambient pressure followed by a smooth metal to insulator transition at 80 K, while the metallic state is stabilized under pressure, a behaviour in strike contrast from the one reported in 1992, since no abrupt decrease of resistivity was noticed in our study. The earlier results might find their interpretation in a current intensity induced melting of a charge order state, in line with our own observation of a current dependent resistivity drop under pressure in one sample possibly mixing in-plane and out-of-plane conductivity. Since this resistivity decrease remains unchanged under magnetic field, it unambiguously indicates that it is not related to a superconducting transition. This result is of utmost importance as it leaves open the quest for the first chiral molecular superconductor and spotlights the research on the growing family of chiral molecular conductors provided with intriguing properties.

Supporting Information

Supporting Information is available from the Wiley Online Library or from the author.

Acknowledgements

This work was supported in France by the ANR (Project 15-CE29-0006-01 ChiraMolCo), the CNRS and the University of Angers. Work in Spain was supported by the Spanish MICIU (Grants PGC2018-096955-B-C44 and PGC2018-093863-B-C22), the MINECO (Grant SEV-

2015-0496 and MDM-2017-0767) and by Generalitat de Catalunya (2017SGR1506 and 2017SGR1289).

Received: ((will be filled in by the editorial staff))
Revised: ((will be filled in by the editorial staff))
Published online: ((will be filled in by the editorial staff))

References

[1] F. Pop, N. Zigon, N. Avarvari, *Chem. Rev.* **2019**, *119*, 8435–8478.

[2] J. D. Dunitz, A. Karrer, J. D. Wallis, *Helv. Chim. Acta* **1986**, *69*, 69–70.

[3] A. Karrer, J. D. Wallis, J. D. Dunitz, B. Hilti, C. W. Mayer, M. Bürkle, J. Pfeiffer, *Helv. Chim. Acta* **1987**, *70*, 942–953.

[4] J. S. Zambounis, C. W. Mayer, *Tetrahedron Lett.* **1991**, *32*, 2737–2740.

[5] S. Matsumiya, A. Izuoka, T. Sugawara, T. Taruishi, Y. Kawada, *Bull. Chem. Soc. Jpn.* **1993**, *66*, 513–522.

[6] S. Matsumiya, A. Izuoka, T. Sugawara, T. Taruishi, Y. Kawada, M. Tokumoto, *Bull. Chem. Soc. Jpn.* **1993**, *66*, 1949–1954.

[7] G. L. J. A. Rikken, J. Fölling, P. Wyder, *Phys. Rev. Lett.* **2001**, *87*, 236602.

[8] V. Krstic, S. Roth, M. Burghard, K. Kern, G. L. J. A. Rikken, *J. Chem. Phys.* **2002**, *117*, 11315–11319.

[9] C. Réthoré, N. Avarvari, E. Canadell, P. Auban-Senzier, M. Fourmigué, *J. Am. Chem. Soc.* **2005**, *127*, 5748–5749.

[10] A. M. Madalan, C. Réthoré, M. Fourmigué, E. Canadell, E. B. Lopes, M. Almeida, P. Auban-Senzier, N. Avarvari, *Chem. Eur. J.* **2010**, *16*, 528–537.

[11] F. Pop, P. Auban-Senzier, E. Canadell, N. Avarvari, *Chem. Commun.* **2016**, *52*, 12438–12441.

[12] N. Avarvari, J. D. Wallis, *J. Mater. Chem.* **2009**, *19*, 4061–4076.

[13] F. Pop, S. Laroussi, T. Cauchy, C. J. Gómez-García, J. D. Wallis, N. Avarvari, *Chirality* **2013**, *25*, 466–474.

[14] J. R. Galán-Mascarós, E. Coronado, P. A. Goddard, J. Singleton, A. I. Coldea, J. D. Wallis, S. J. Coles, A. Alberola, *J. Am. Chem. Soc.* **2010**, *132*, 9271–9273.

[15] S. Yang, F. Pop, C. Melan, A. C. Brooks, L. Martin, P. Horton, P. Auban-Senzier, G. L. J. A. Rikken, N. Avarvari, J. D. Wallis, *CrystEngComm* **2014**, *16*, 3906–3916.

[16] M. Atzori, F. Pop, P. Auban-Senzier, R. Clérac, E. Canadell, M. L. Mercuri, N. Avarvari, *Inorg. Chem.* **2015**, *54*, 3643–3653.

[17] S. J. Krivickas, A. Ichikawa, K. Takahashi, H. Tajima, J. D. Wallis, H. Mori, *Synth. Met.* **2011**, *161*, 1563–1565.

[18] F. Pop, M. Allain, P. Auban-Senzier, J. Martínez-Lillo, F. Lloret, M. Julve, E. Canadell, N. Avarvari, *Eur. J. Inorg. Chem.* **2014**, 3855–3862.

[19] F. Pop, P. Auban-Senzier, A. Frąckowiak, K. Ptaszyński, I. Olejniczak, J. D. Wallis, E. Canadell, N. Avarvari, *J. Am. Chem. Soc.* **2013**, *135*, 17176–17186.

[20] N. Mroweh, P. Auban-Senzier, N. Vanthuyne, E. Canadell, N. Avarvari, *J. Mater. Chem. C* **2019**, *7*, 12664–12673.

[21] F. Pop, P. Auban-Senzier, E. Canadell, G. L. J. A. Rikken, N. Avarvari, *Nat. Commun.* **2014**, *5*, 3757.

[22] F. Qin, W. Shi, T. Ideue, M. Yoshida, A. Zak, R. Tenne, T. Kikitsu, D. Inoue, D. Hashizume, Y. Iwasa, *Nat. Commun.* **2017**, *8*, 14465.

[23] R. Wakatsuki, Y. Saito, S. Hoshino, Y. M. Itahashi, T. Ideue, M. Ezawa, Y. Iwasa, N. Nagaosa, *Sci. Adv.* **2017**, *3*, e1602390.

[24] T. Kvorning, T. H. Hansson, A. Quelle, C. Morais Smith, *Phys. Rev. Lett.* **2018**, *120*, 217002.

[25] M. Claassen, D. M. Kennes, M. Zingl, M. A. Sentef, A. Rubio, *Nat. Phys.* **2019**, *15*, 766–770.

[26] M. Smidman, M. B. Salamon, H. Q. Yuan, D. F. Agterberg, *Rep. Prog. Phys.* **2017**, *80*, 036501.

[27] E. M. Carnicom, W. Xie, T. Klimczuk, J. Lin, K. Górnicka, Z. Sobczak, N. P. Ong, R. J. Cava, *Sci. Adv.* **2018**, *4*, eaar7969.

[28] J. Wosnitza, *Crystals* **2012**, *2*, 248–265.

[29] J. S. Zambounis, C. W. Mayer, K. Hauenstein, B. Hilti, W. Hofherr, J. Pfeiffer, M. Bürkle, G. Rihs, *Adv. Mater*. **1992**, *4*, 33–35.

[30] J. A. Schlueter, U. Geiser, M. A. Whited, N. Drichko, B. Salameh, K. Petukhov, M. Dressel, *Dalton Trans.* **2007**, 2580–2588.

[31] T. G. Prokhorova, L. I. Buravov, E. B. Yagubskii, L. V. Zorina, S. V. Simonov, R. P. Shibaeva, V. N. Zverev, *Eur. J. Inorg. Chem.* **2014**, 3933–3940.

[32] A. A. Galimzyanov, A. A. Ignat'ev, N. D. Kushch, V. N. Laukhin, M. K. Makova, V. A. Merzhanov, L. P. Rozenberg, R. P. Shibaeva, E. B. Yagubskii, *Synth. Met.* **1989**, *33*, 81–91.

[33] V. E. Korotkov, V. N. Molchanov, R. P. Shibaeva, *Sov. Phys. Crystallogr.* **1992**, *37*, 776–782.

[34] M.-L. Doublet, E. Canadell, R. P. Shibaeva, *J. Phys. I France* **1994**, *4*, 1479–1490.

[35] M.-H. Whangbo, J. M. Williams, P. C. W. Leung, M. A. Beno, T. J. Emge, H. H. Wang, *Inorg. Chem*. **1985**, *24*, 3500–3502.

[36] V. N. Zverev, M. V. Kartsovnik, W. Biberacher, S. S. Khasanov, R. P. Shibaeva, L. Ouahab, L. Toupet, N. N. Kushch, E. B. Yagubskii, E. Canadell, *Phys. Rev. B* **2010**, *82*, 155123.

[37] W. Kaddour, P. Auban-Senzier, H. Raffy, M. Monteverde, J.-P. Pouget, C. R. Pasquier, P. Alemany, E. Canadell, L. Valade, *Phys. Rev. B* **2014**, *90*, 205132.

[38] F. Sawano, I. Terasaki, H. Mori, T. Mori, M. Watanabe, N. Ikeda, Y. Nogami, Y. Noda, *Nature* **2005**, *437*, 522–524.

[39] M. Watanabe, K. Yamamoto, T. Ito, Y. Nakashima, M. Tanabe, N. Hanasaki, N. Ikeda, Y. Nogami, H. Ohsumi, H. Toyokawa, Y. Noda, I. Terasaki, F. Sawano, T. Suko, H. Mori, T. Mori, *J. Phys. Soc. Jpn.* **2008**, *77*, 065004.

[40] H. Endo, T. Kawamoto, T. Mori, I. Terasaki, T. Kakiuchi, H. Sawa, M. Kodani, K. Takimiya, T. Otsubo, *J. Am. Chem. Soc.* **2006**, *128*, 9006–9007.

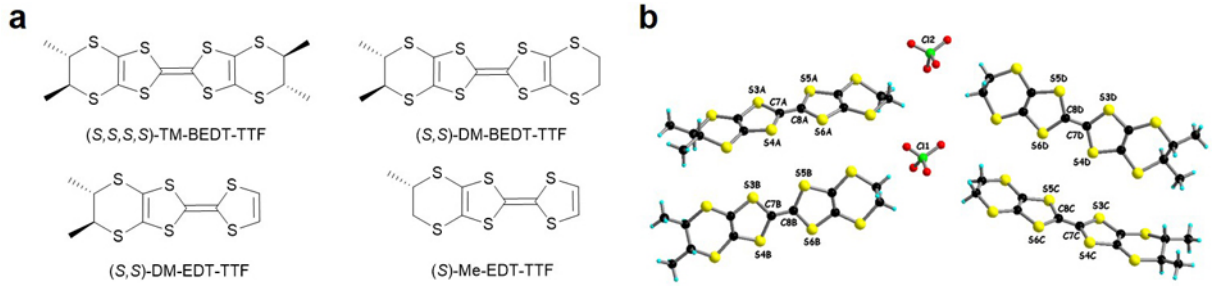

Figure 1. a) Enantiopure BEDT-TTF and EDT-TTF based donors including DM-BEDT-TTF, involved in this study. b) Crystalline structure of κ-[(*R*,*R*)-DM-BEDT-TTF]$_2$ClO$_4$ highlighting the four independent donors and two anions in the asymmetric unit.

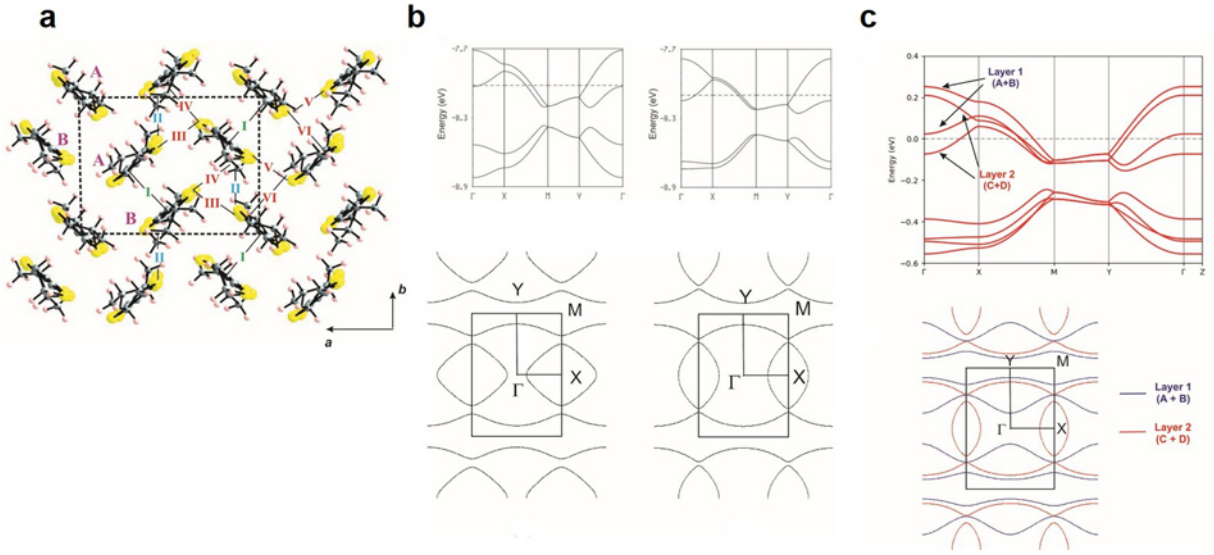

Figure 2. a) Donor layer 1 of the κ-[(*R*,*R*)-DM-BEDT-TTF]$_2$ClO$_4$ and κ-[(*S*,*S*)-DM-BEDT-TTF]$_2$ClO$_4$ salts where the different donors and intermolecular interactions are labelled. b) (top panels) Extended Hückel band structure for the two donor layers of κ-[(*R*,*R*)-DM-BEDT-TTF]$_2$ClO$_4$: (left) layer type 1, and (right) layer type 2. The dashed line refers to the calculated Fermi level assuming two holes per layer. Γ = (0, 0), X = (*a**/2, 0), Y = (0, *b**/2), M = (*a**/2, *b**/2) and S = (-*a**/2, *b**/2). (bottom panels) Extended Hückel Fermi surface for the two donor layers of κ-[(*R*,*R*)-DM-BEDT-TTF]$_2$ClO$_4$ assuming an equal partition of holes between the two layers: (left) layer type 1, and (right) layer type 2. c) DFT electronic structure of the κ-[(*R*,*R*)-DM-BEDT-TTF]$_2$ClO$_4$ salt: (top) Band structure where the dashed line refers to the Fermi level and Γ = (0, 0, 0), X = (1/2, 0, 0), Y = (0, 1/2, 0), M = (1/2, 1/2, 0) and Z = (0, 0, 1/2) in units of the reciprocal lattice vectors. The partially filled bands associated with the two types of layers are labelled; (bottom) Fermi surface (section for *c** = 0.0) where the blue and red contributions are those of layers 1 and 2, respectively.

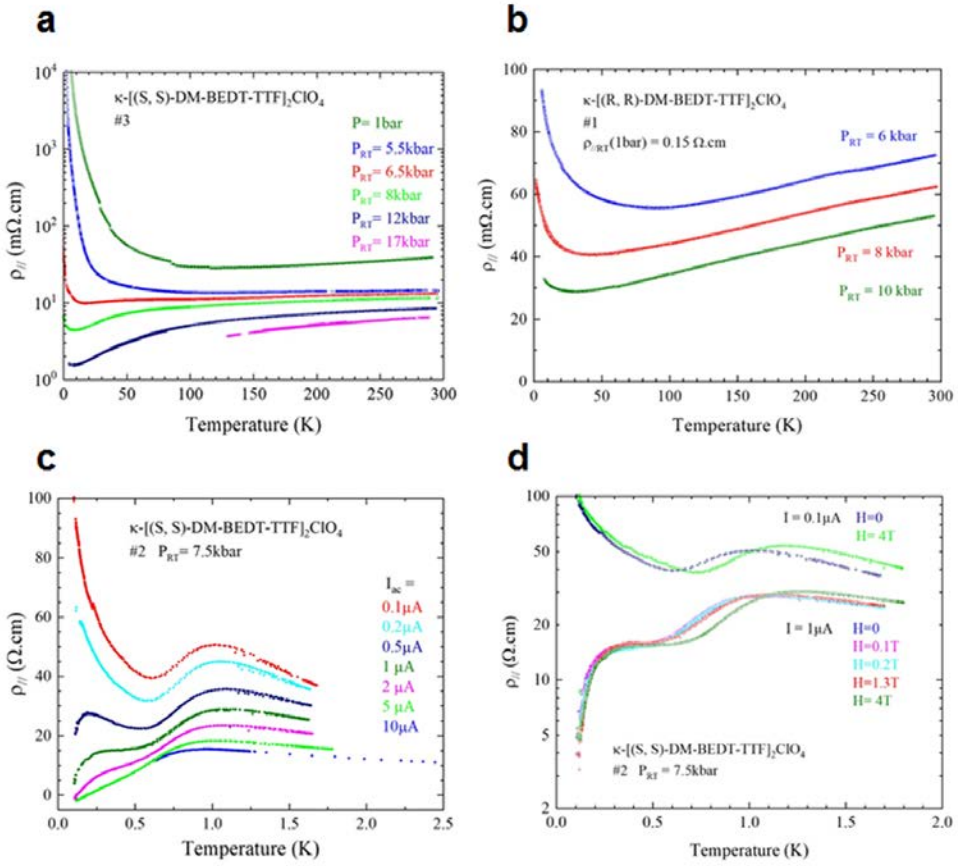

Figure 3. Temperature dependence of the in-plane electrical resistivity $\rho_{//}$ for a single crystal of κ-[(*S*,*S*)-DM-BEDT-TTF]$_2$ClO$_4$ (a) and for a single crystal of κ-[(*R*,*R*)-DM-BEDT-TTF]$_2$ClO$_4$ (b) at different pressures. c) Temperature dependence of the electrical resistivity ρ for a single crystal (#2) of κ-[(*S*,*S*)-DM-BEDT-TTF]$_2$ClO$_4$ in 4 points for different current intensities and under an applied pressure of 7.5 kbar. It shows a current induced insulator to metal transition below 1 K. d) Temperature dependence below 2 K of the in-plane electrical resistivity for a single crystal of κ-[(*S*,*S*)-DM-BEDT-TTF]$_2$ClO$_4$ (#2) at 7.5 kbar plotted for two different applied currents and different magnetic fields applied perpendicularly to the (*a*,*b*) plane.

Table 1. Absolute values of the $\beta_{HOMO-HOMO}$ interaction energies[35] (eV) for the different donor···donor interactions in the [(*R*,*R*)-DM-BEDT-TTF]$_2$ClO$_4$ and [(*S*,*S*)-DM-BEDT-TTF]$_2$ClO$_4$ salts.

Interaction	**(*R*,*R*)**		**(*S*,*S*)**	
	Layer 1 (A-B)	**Layer 2 (C-D)**	**Layer 1 (A-B)**	**Layer 2 (C-D)**
I	0.4067	0.3996	0.4059	0.3996
II	0.2453	0.1967	0.2419	0.1954
III	0.1371	0.0727	0.1298	0.0725
IV	0.0199	0.0635	0.0232	0.0584
V	0.0672	0.0466	0.0623	0.0481
VI	0.0248	0.0729	0.0282	0.0747

The enantiopure mixed valence radical cations salts κ-[(*S*,*S*)-DM-BEDT-TTF]$_2$ClO$_4$ and κ-[(*R*,*R*)-DM-BEDT-TTF]$_2$ClO$_4$, prepared by electrocrystallization of the chiral donor DM-BEDT-TTF, show metallic conductivity but no superconducting transition, unlike the conclusions of an earlier report. Original structural and electronic features consisting in two different κ-type layers having 1D and 2D electronic dimensionality are revealed by structural investigations and band structure calculations.

Chiral conductors

N. Mroweh, C. Mézière, F. Pop,* P. Auban-Senzier, P. Alemany, E. Canadell,* N. Avarvari*

In search of chiral molecular superconductors: κ-[(*S*,*S*)-DM-BEDT-TTF]$_2$ClO$_4$ revisited

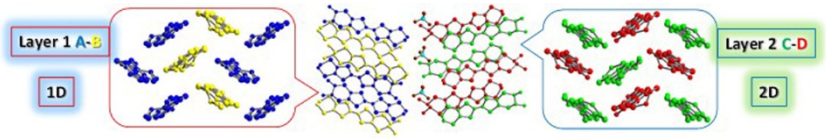

Supporting Information

In search of chiral molecular superconductors: κ-[(*S,S*)-DM-BEDT-TTF]$_2$ClO$_4$ revisited

Nabil Mroweh, Cécile Mézière, Flavia Pop, Pascale Auban-Senzier, Pere Alemany, Enric Canadell,* and Narcis Avarvari**

Experimental section

Electrocrystallization

Dark black plate-like single crystals of κ-[(*S*,*S*)-DM-BEDT-TTF]$_2$ClO$_4$ and κ-[(*R*,*R*)-DM-BEDT-TTF]$_2$ClO$_4$ were obtained by electrocrystallization. The electrolyte solution was prepared from 20 mg (5 eq.) of [NBu$_4$]ClO$_4$ dissolved in 12 mL of tetrahydrofuran. The anodic chamber was filled with 5 mg of the corresponding donor dissolved in 6 mL of the previously prepared electrolyte solution, whereas the rest of the electrolyte solution (6 ml) was added in the cathodic compartment of the electrocrystallization cell. Single crystals, as black crystalline plates, of the salt were grown at 2-3 °C over a period of 10 days on a platinum wire electrode by applying a constant current of 0.5 μA.

X-Ray structure determinations

Details about data collection and solution refinement are given in Table S1. Single crystals of the compounds were mounted on glass fibre loops using a viscous hydrocarbon oil to coat the crystal and then transferred directly to cold nitrogen stream for data collection. X-ray data collection were performed at 150 K on an Agilent Supernova with CuKα (λ = 1.54184 Å) and at 293 K on a Nonius Kappa CCD diffractometer, using graphite-monochromated MoK_α radiation (λ = 0.71073 Å). The structures were solved by direct methods with the SHELXS-97 and SIR92 programs and refined against all F_2 values with the SHELXL-97 program[1] using the WinGX graphical user interface.[2]. All non-H atoms were refined anisotropically. Hydrogen atoms were introduced at calculated positions (riding model), included in structure factor calculations but not refined.

Crystallographic data for the two structures obtained at 150 K have been deposited with the Cambridge Crystallographic Data Centre, deposition numbers CCDC 1999140 for κ-[(*R*,*R*)-DM-BEDT-TTF]$_2$ClO$_4$ and CCDC 1999141 for κ-[(*S*,*S*)-DM-BEDT-TTF]$_2$ClO$_4$. These data can be obtained free of charge from CCDC, 12 Union road, Cambridge CB2 1EZ, UK (e-mail: deposit@ccdc.cam.ac.uk or http://www.ccdc.cam.ac.uk).

[1] G. M. Sheldrick, *Programs for the Refinement of Crystal Structures,* ed. **1996**

[2] L. Farrugia, *Journal of applied crystallography* **1999**, *32*, 837.

Table S1. Crystal Data and Structure Refinement for κ-[(*S*,*S*)-DM-BEDT-TTF]$_2$ClO$_4$ and κ-[(*R*,*R*)-DM-BEDT-TTF]$_2$ClO$_4$, both at *r.t.* and 150 K.

Compound	κ-[(*S*,*S*)-DM-BEDT-TTF]$_2$ClO$_4$	κ-[(*S*,*S*)-DM-BEDT-TTF]$_2$ClO$_4$	κ-[(*R*,*R*)-DM-BEDT-TTF]$_2$ClO$_4$	κ-[(*R*,*R*)-DM-BEDT-TTF]$_2$ClO$_4$
Empirical formula	C_{48} H_{48} Cl_2 O_8 S_{32}	C_{48} H_{48} Cl_2 O_8 S_{32}	C_{48} H_{48} Cl_2 O_8 S_{32}	C_{48} H_{48} Cl_2 O_8 S_{32}
Fw	1849.68	1849.68	1849.68	1849.68
***T* (K)**	293(2)	150.00(10)	293(2)	150(2)
Wavelength (Å)	0.71073	1.54184	0.71073	1.54184
Cryst syst	Monoclinic	Monoclinic	Monoclinic	Monoclinic
Space group	$P2_1$	$P2_1$	$P2_1$	$P2_1$
***a* (Å)**	11.9422(15)	11.71267(19)	11.9241(16)	11.7065(2)
***b* (Å)**	8.5246(11)	8.46218(13)	8.5246(4)	8.45970(10)
***c* (Å)**	34.948(2)	34.8155(5)	34.915(2)	34.8134(4)
α(deg)	90	90	90	90
β(deg)	93.369(7)	93.6984(14)	93.393(9)	93.7240(10)
γ(deg)	90	90	90	90
***V* (Å^3)**	3551.6(7)	3443.54(9)	3542.8(6)	3440.41(8)
Z	2	2	2	2
***D*$_c$ (g cm^{-3})**	1.730	1.784	1.734	1.786
Abs coeff (mm^{-1})	1.082	10.355	1.085	10.365
Cryst size (mm^3)	0.3 x 0.3 x 0.02	0.3 x 0.3 x 0.02	0.3 x 0.3 x 0.02	0.236 x 0.164 x 0.035
Flack parameter	0.02(14)	0.070(13)	0.02(6)	0.024(10)
GOF on *F*^{2}	1.036	1.077	0.979	1.016
Final *R* indices [*I* > 2σ(*I*)][a]	0.0714/0.1671	0.0507/0.1281	0.0507/0.1365	0.0340/0.0848
***R* indices (all data)**[a]	0.1623/0.2068	0.0524/0.1299	0.1305/0.1837	0.0360/0.0864

[a] $R(F_o) = \Sigma||F_o| - |F_c||/\Sigma|F_o|$; $R_w(F_o^2) = [\Sigma[w(F_o^2 - F_c^2)^2]/\Sigma[w(F_o^2)^2]]^{1/2}$

Compound κ-[(*S*,*S*)-DM-BEDT-TTF]$_2$ClO$_4$

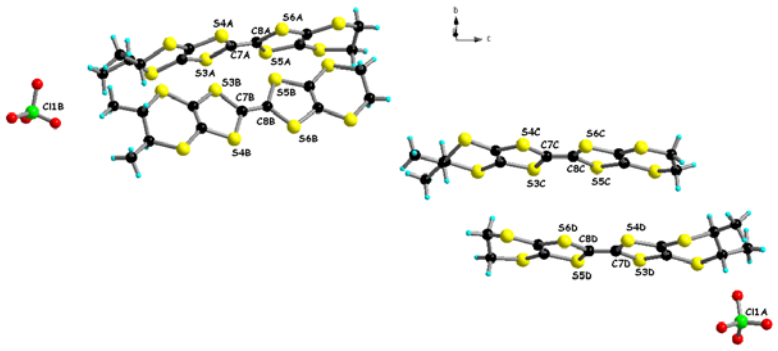

Figure S1. Crystalline structure of κ-[(*S*,*S*)-DM-BEDT-TTF]$_2$ClO$_4$ highlighting the four independent donors and two anions in the asymmetric unit.

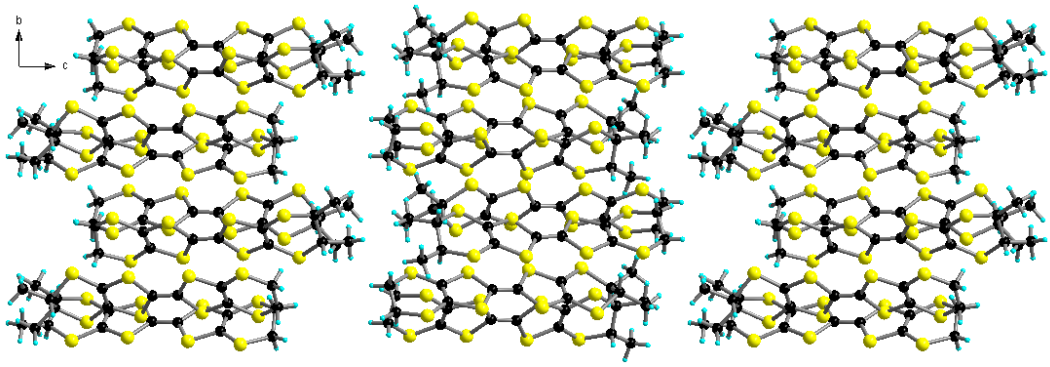

Figure S2. Crystalline packing of κ-[(*S*,*S*)-DM-BEDT-TTF]$_2$ClO$_4$ in the *bc* plane. ClO$_4$ anions have been omitted.

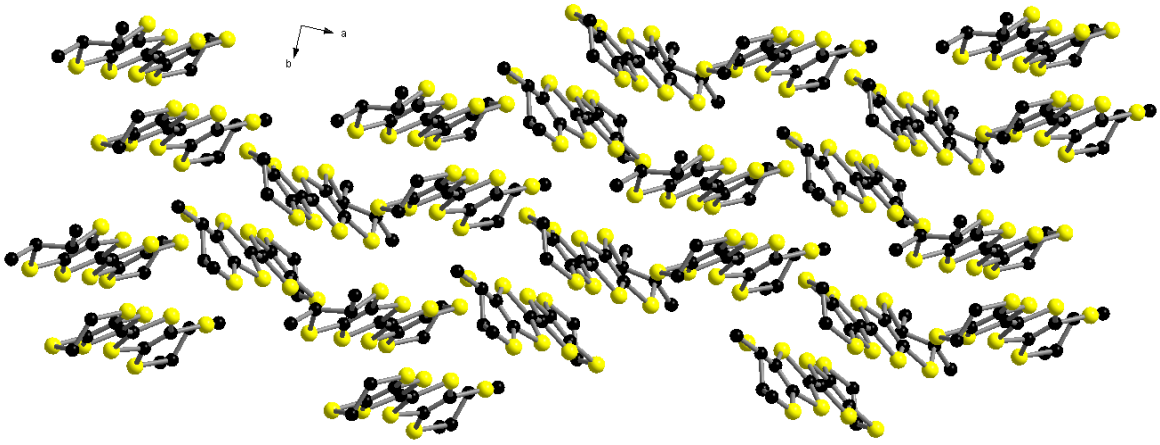

Figure S3. Crystalline packing of κ-[(*S*,*S*)-DM-BEDT-TTF]$_2$ClO$_4$ in the conducting *ab* plane. ClO$_4$ anions have been omitted.

Compound κ-[(*R*,*R*)-DM-BEDT-TTF]$_2$ClO$_4$

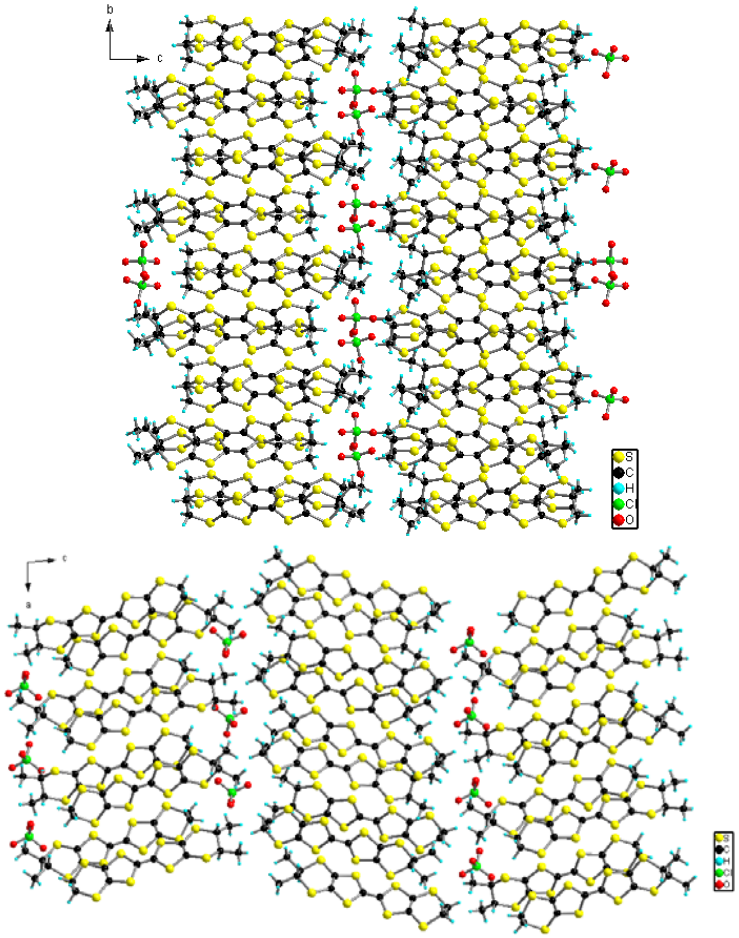

Figure S4. Crystalline packing of κ-[(*R*,*R*)-DM-BEDT-TTF]$_2$ClO$_4$ in the *bc* (top) and *ac* (bottom) planes.

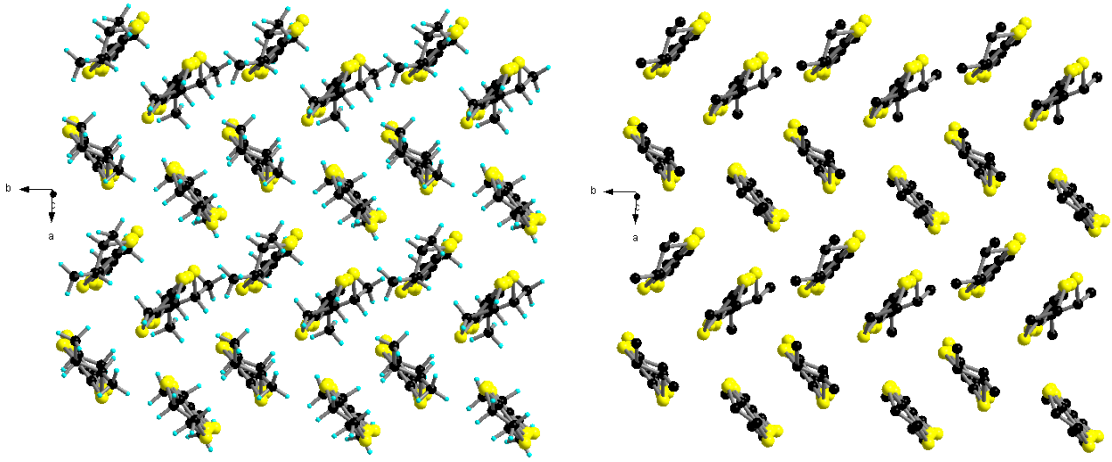

Figure S5. Crystalline packing of κ-[(*R*,*R*)-DM-BEDT-TTF]$_2$ClO$_4$ in the conducting *ab* plane; H atoms (left), no H-atoms (right).

Table S2. Selected bond lengths (Å) for κ-[(*S*,*S*)-DM-BEDT-TTF]$_2$ClO$_4$ and κ-[(*R*,*R*)-DM-BEDT-TTF]$_2$ClO$_4$ at 150 K.

κ-[(S,S)-DM-BEDT-TTF]$_2$ClO$_4$			κ-[(R,R)-DM-BEDT-TTF]$_2$ClO$_4$		
Molecule	C═C (Å)	C–S (Å)	Molecule	C═C (Å)	C–S (Å)
A	1.3540(98)	1.7438(84)	A	1.3581(73)	1.7269(49)
		1.7480(87)			1.7501(51)
		1.7587(86)			1.7435(61)
		1.7308(83)			1.7414(56)
B	1.3586(99)	1.7428(86)	B	1.3553(76)	1.7423(60)
		1.7527(94)			1.7302(56)
		1.7368(87)			1.7365(56)
		1.7418(83)			1.7524(61)
C	1.3512(148)	1.7546(91)	C	1.3560(65)	1.7576(49)
		1.7257(95)			1.736(5)
		1.7300(99)			1.7401(51)
		1.7552(100)			1.7477(49)
D	1.3891(149)	1.7251(99)	D	1.3538(67)	1.7481(49)
		1.7317(99)			1.7455(51)
		1.7306(99)			1.7313(51)
		1.7391(99			1.7538(49)

Band structure calculations

Computational details

The tight-binding band structure calculations were of the extended Hückel type.[1] A modified Wolfsberg-Helmholtz formula was used to calculate the non-diagonal $H_{\mu\nu}$ values.[2] All valence electrons were taken into account in the calculations and the basis set consisted of Slater-type orbitals of double-ζ quality for C 2s and 2p, S 3s and 3p and of single-ζ quality for H 1s. The ionization potentials, contraction coefficients and exponents were taken from previous work.[3]

The first-principles calculations were carried out using a numerical atomic orbitals density functional theory (DFT) approach[4,5] which was developed for efficient calculations in large systems and implemented in the SIESTA code.[6-8] We have used the generalized gradient approximation (GGA) to DFT and, in particular, the functional of Perdew, Burke and Ernzerhof.[9] Only the valence electrons are considered in the calculation, with the core being replaced by norm-conserving scalar relativistic pseudopotentials[10] factorized in the Kleinman-Bylander form.[11] We have used a split-valence double-ζ basis set including polarization orbitals with an energy shift of 10 meV for all atoms.[12] The energy cutoff of the real space integration mesh was 250 Ry. The Brillouin zone was sampled using a grid of (20×20×5) k-points[13] in the irreducible part of the Brillouin zone. The experimental crystal structures were used for the calculations.

References

1. Whangbo, M.-H.; Hoffmann, R. *J. Am. Chem. Soc.* **1978**, *100*, 6093-6098.
2. Ammeter, J. H.; Bürgi, H.-B.; Thibeault, J.; Hoffmann, R. *J. Am. Chem. Soc.* **1978**, *100*, 3686-3692.
3. Pénicaud, A.; Boubekeur, K.; Batail, P.; Canadell, E.; Auban-Senzier, P.; Jérome, D. *J. Am. Chem. Soc.* **1993**, *115*, 4101-4112.
4. Hohenberg, P.; Kohn W. *Phys. Rev.* **1965**, *136*, B864-B871.
5. Kohn W.; Sham L. J. *Phys. Rev.* **1965**, *140*, A1133-A1138.
6. Soler J. M.; Artacho E.; Gale J. D.; García A.; Junquera J.; Ordejón P.; Sánchez-Portal D. *J. Phys.: Condens. Matter.* **2002**, *14*, 2745-2779.
7. Artacho E.; Anglada E.; Diéguez O.; Gale J. D.; García A.; Junquera J.; Martin R. M.; Ordejón P.; Pruneda J. M.; Sánchez-Portal D.; Soler J. M. *J. Phys.: Condens. Matter*. **2008**, *20*, 064208.
8. For more information on the SIESTA code visit: http://departments.icmab.es/leem/siesta/
9. Perdew J. P.; Burke K.; Ernzerhof M. *Phys. Rev. Lett.* **1966**, *77*, 3865-3868.
10. Troullier N.; Martins J. L. *Phys. Rev. B* **1991**, *43*, 1993-2006.
11. Kleinman L.; Bylander D. M. *Phys. Rev. Lett.* **1982**, *48*, 1425-1428.
12. Artacho E.; Sánchez-Portal D.; Ordejón P.; García A.; and Soler J. M. *Phys. Stat. Sol. (b)* **1999**, *215*, 809-817.
13. Monkhorst H. J.; Pack J. D. *Phys. Rev. B*, **1976**, *13*, 5188-5192.

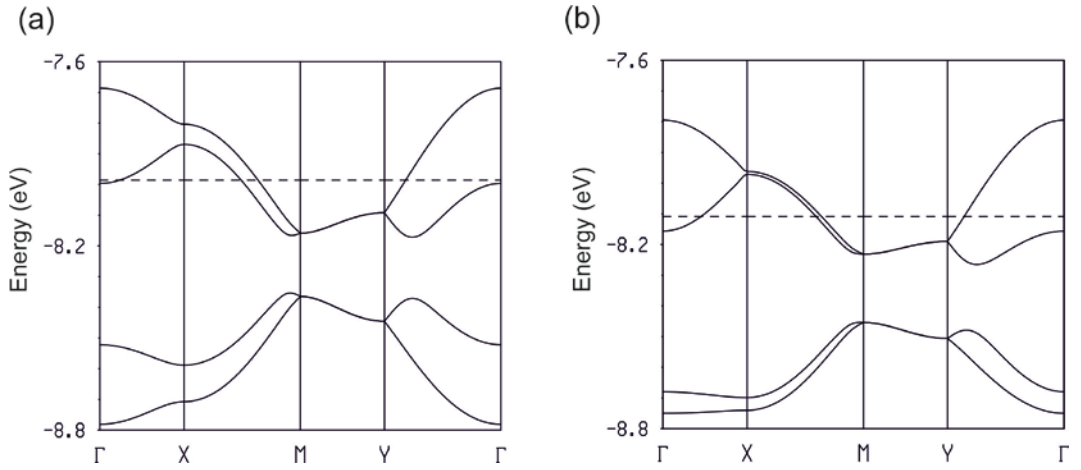

Figure S6. Extended Hückel band structure for the two donor layers of κ-[(*S*,*S*)-DM-BEDT-TTF]$_2$ClO$_4$: (a) layer type 1, and (b) layer type 2. The dashed line refers to the calculated Fermi level assuming two holes per layer. Γ = (0, 0), X = (*a**/2, 0), Y = (0, *b**/2), M = (*a**/2, *b**/2) and S = (-*a**/2, *b**/2).

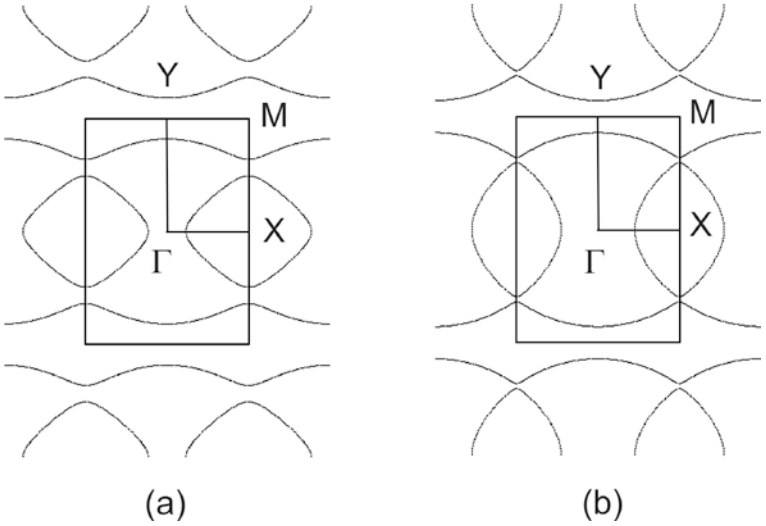

Figure S7. Extended Hückel Fermi surface for the two donor layers of κ-[(*S*,*S*)-DM-BEDT-TTF]$_2$ClO$_4$ assuming an equal partition of holes between the two layers: (a) layer type 1, and (b) layer type 2.

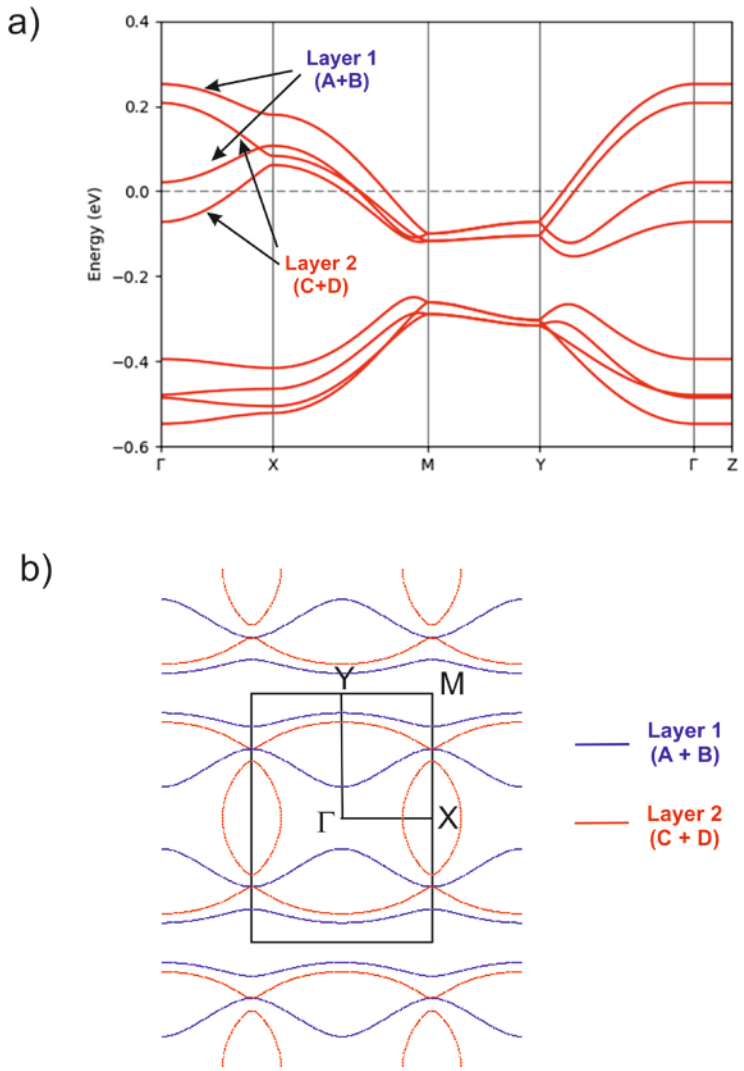

Figure S8. DFT electronic structure of the κ-[(*S*,*S*)-DM-BEDT-TTF]$_2$ClO$_4$ salt: (a) Band structure where the dashed line refers to the Fermi level and Γ = (0, 0, 0), X = (1/2, 0, 0), Y = (0, 1/2, 0), M = (1/2, 1/2, 0) and Z = (0, 0, 1/2) in units of the reciprocal lattice vectors. The partially filled bands associated with the two types of layers are labelled; (b) Fermi surface (section for c^* = 0.0) where the blue and red contributions are those of layers 1 and 2, respectively.

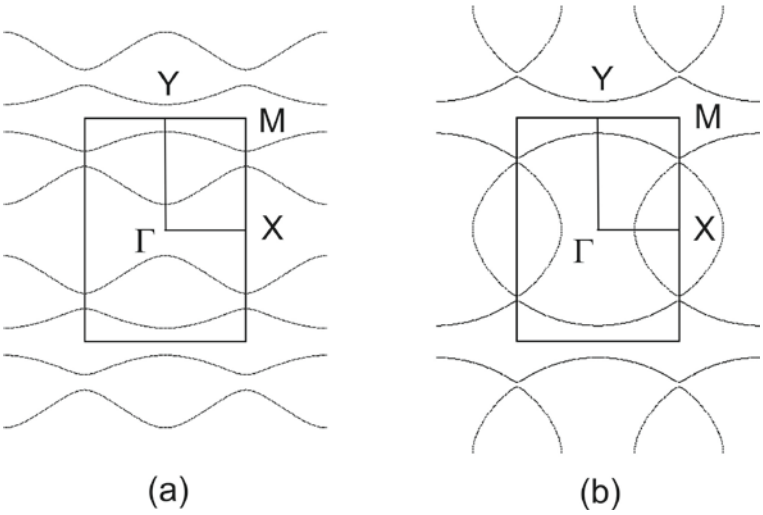

Figure S9. Extended Hückel Fermi surface for the two donor layers of κ-[(*S*,*S*)-DM-BEDT-TTF]$_2$ClO$_4$ where the DFT hole transfer between the two layers is taken into account: (a) layer type 1, and (b) layer type 2.

Conductivity measurements

Electrical resistivity was measured on platelet-shaped single crystals of both enantiomers using a four-point method. Four aligned gold contacts were evaporated on both large faces of the crystals for the in-plane configuration and two gold contacts were evaporated on each large face of the crystals for the out-of-plane configuration. Gold wires were glued with silver paste on those contacts. A low-frequency (<100 Hz) lock-in technique was used with a measuring current I_{ac} = 10 μA. Lower values down to 0.1 μA were used for out-of-plane measurements and the non-linearity study in #2 of (*S*,*S*) enantiomer.

Resistivity measurements were also performed under high hydrostatic pressure in homemade clamped cells either a CuBe one up to 12 kbar or a NiCrAl one up to 20 kbar. The pressure is measured at room temperature when the pressure is varied using a manganin gauge and silicon oil (Daphne 7373) is used as the pressure transmitting medium. The loss of pressure during cooling is estimated to 2 kbar between 300 and 50 K, however the pressure indicated in the figures is the pressure measured at room temperature.

Resistivity measurements have been performed in the temperature range 4−300 K using a cryostat equipped with a 4 K pulse-tube (out-of-plane measurements, #1 of (*S*,*S*) enantiomer and (*R*,*R*) enantiomer) and in a dilution refrigerator down to 100 mK for the highest-pressure experiments (#2 and #3 of (*S*,*S*) enantiomer) equipped with a superconducting coil for generating the magnetic field.

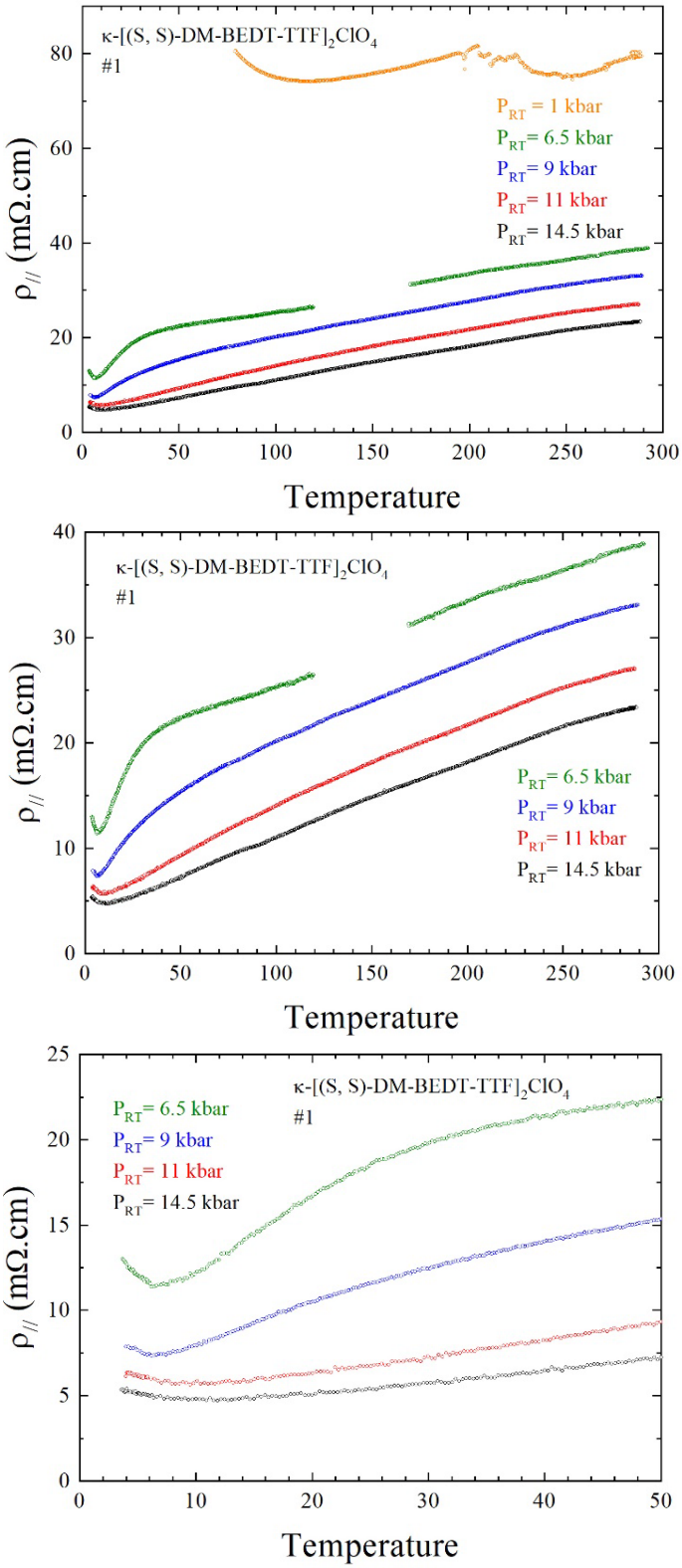

Figure S10. Temperature dependence of the in-plane electrical resistivity $\rho_{//}(T)$ for a single crystal of κ-[(*S*,*S*)-DM-BEDT-TTF]$_2$ClO$_4$ (#1) at different pressures, in the whole measured temperature range (two upper graphs) and below 50 K (bottom).

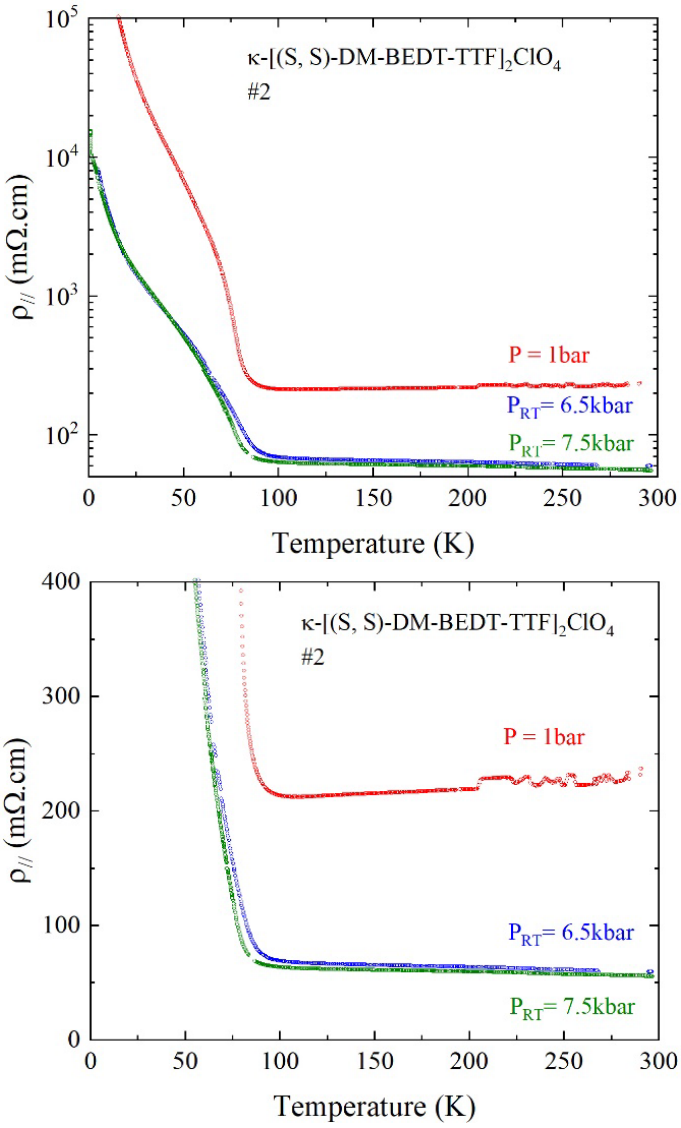

Figure S11. Temperature dependence of the in-plane electrical resistivity $\rho_{//}(T)$ for a single crystal of κ-[(*S*,*S*)-DM-BEDT-TTF]$_2$ClO$_4$ (#2) at different pressures.

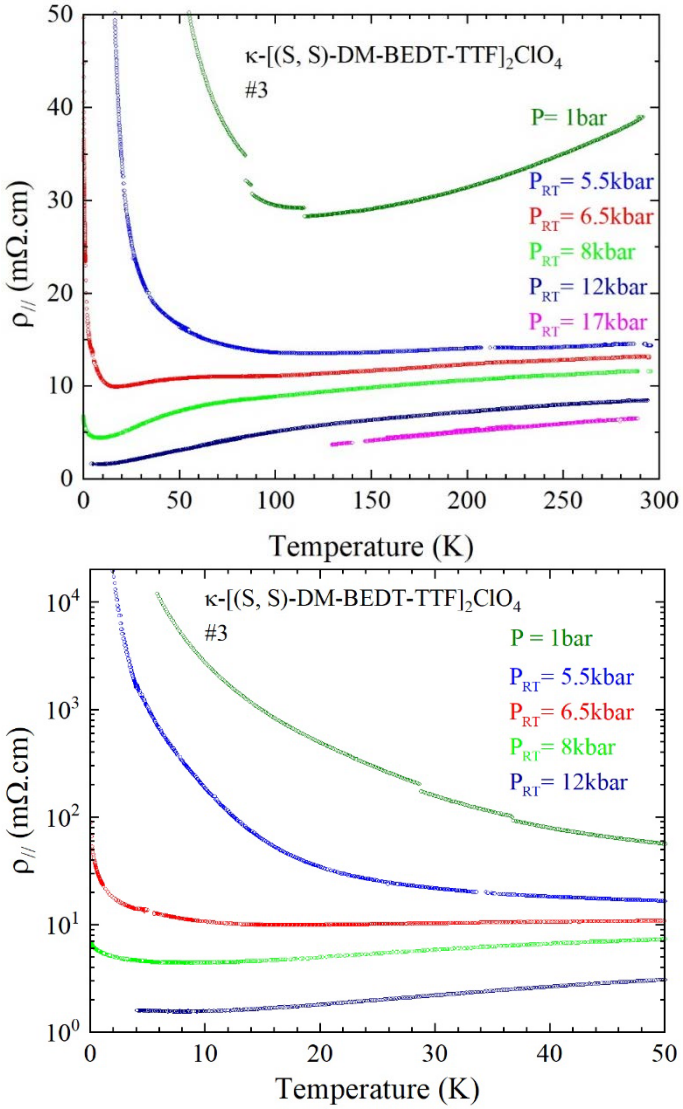

Figure S12. Temperature dependence of the in-plane electrical resistivity $\rho_{//}(T)$ for a single crystal of κ-[(*S*,*S*)-DM-BEDT-TTF]$_2$ClO$_4$ (#3) at different pressures, in the whole measured temperature range (top) and below 50 K (bottom).

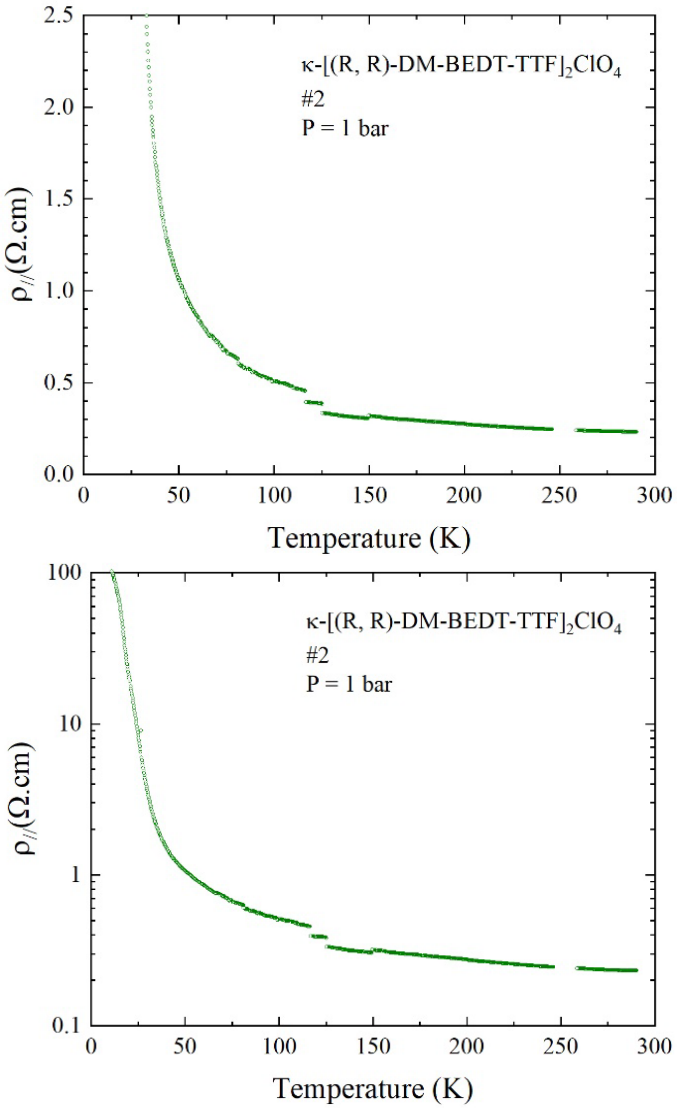

Figure S13. Temperature dependence of the in-plane electrical resistivity $\rho_{//}(T)$ for a single crystal of κ-[(*R*,*R*)-DM-BEDT-TTF]$_2$ClO$_4$ (#2) at P = 1 bar in linear (top) and logarithmic (bottom) vertical scale.

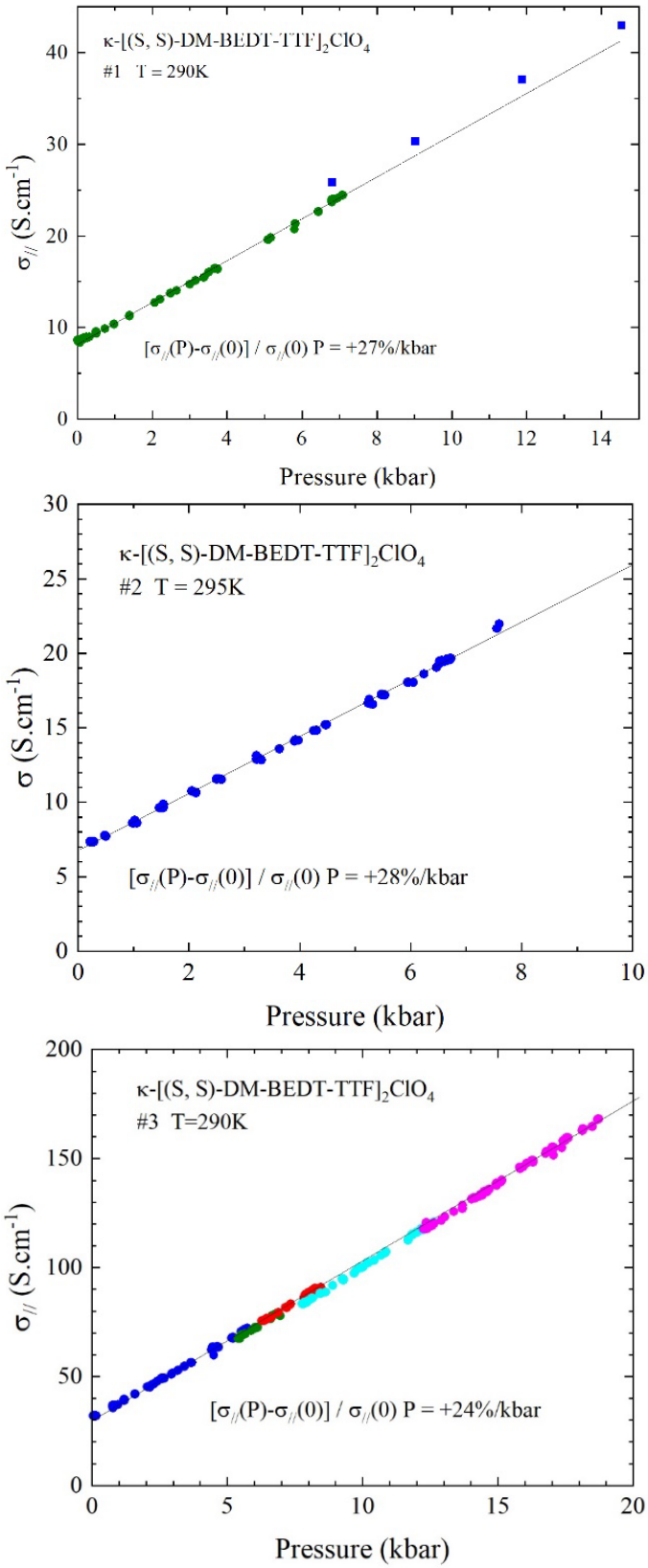

Figure S14. Pressure dependence of the in-plane electrical conductivity at room temperature for the three single crystals of κ-[(*S*,*S*)-DM-BEDT-TTF]$_2$ClO$_4$ measured under pressure. The black line is the linear fit to the data.

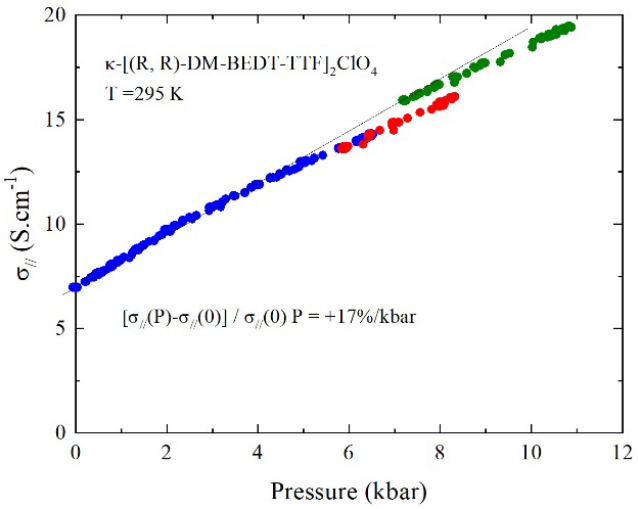

Figure S15. Pressure dependence of the in-plane electrical conductivity at room temperature for a single crystal of κ-[(*R*,*R*)-DM-BEDT-TTF]$_2$ClO$_4$ (#1). The black line is the linear fit to the data.

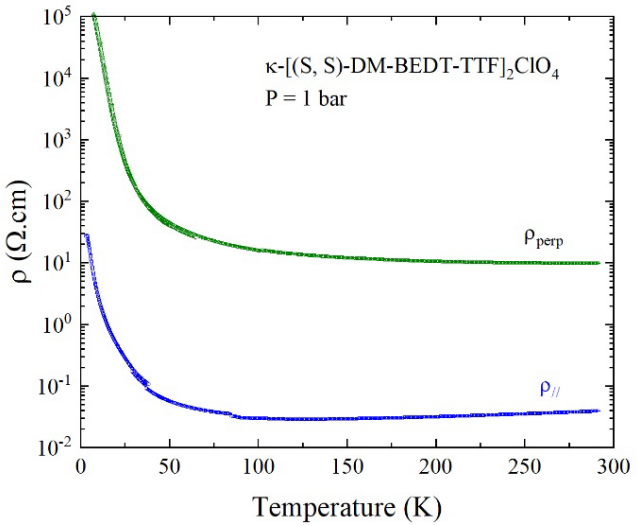

Figure S16. Temperature dependence of the in-plane $\rho_{//}$ and out-of-plane ρ_{perp} electrical resistivity for single crystals of κ-[(*S*,*S*)-DM-BEDT-TTF]$_2$ClO$_4$ at ambient pressure.

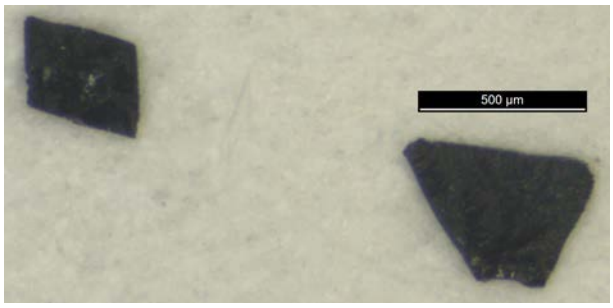

Figure S17. Picture of the black crystalline plates of κ-[(*S*,*S*)-DM-BEDT-TTF]$_2$ClO$_4$.

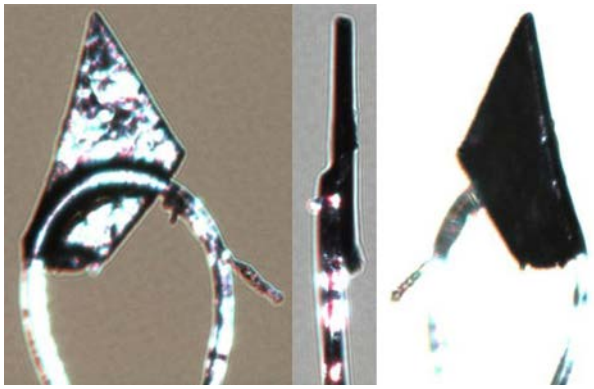

Figure S18. Different views of the measured single crystal of κ-[(*S*,*S*)-DM-BEDT-TTF]$_2$ClO$_4$ mounted on a loop fiber in fomblin oil.

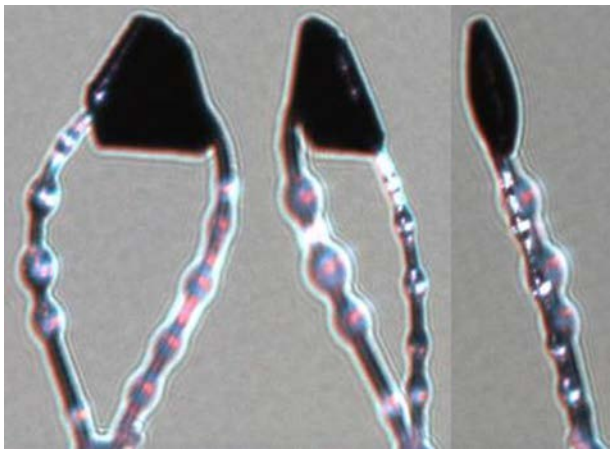

Figure S19. Different views of the measured single crystal of κ-[(*R*,*R*)-DM-BEDT-TTF]$_2$ClO$_4$ mounted on a loop fiber in fomblin oil.

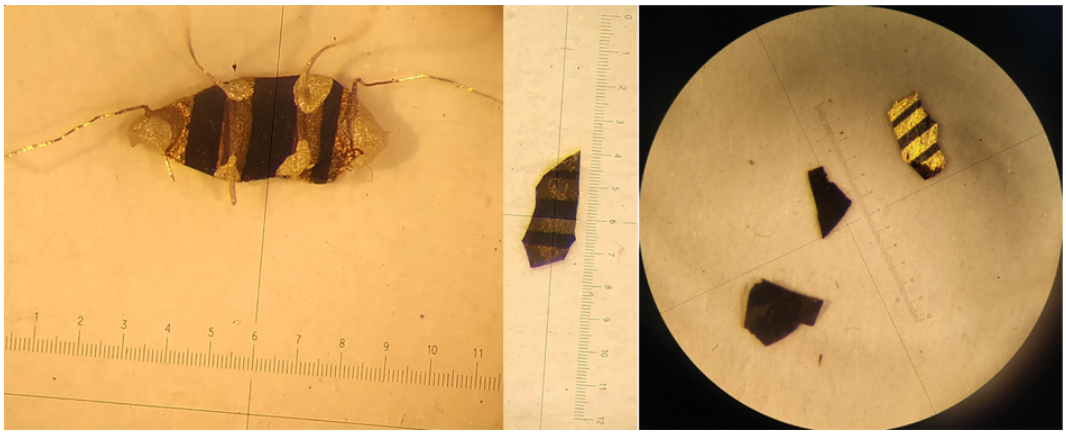

Figure S20. Millimeter size single crystalline plates of κ-[(*S*,*S*)-DM-BEDT-TTF]$_2$ClO$_4$ for single crystal resistivity measurements.

Figure S21. Millimeter size single crystalline plates of κ-[(*R*,*R*)-DM-BEDT-TTF]$_2$ClO$_4$ for single crystal resistivity measurements.